AAC Journals.ASM.org

Antibacterial Properties of Magnesium *In Vitro* and in an *In Vivo* Model of Implant-Associated Methicillin-Resistant *Staphylococcus aureus* Infection

Yang Li,[a] Guangwang Liu,[b] Zanjing Zhai,[a] Lina Liu,[c] Haowei Li,[a] Ke Yang,[d] Lili Tan,[d] Peng Wan,[d] Xuqiang Liu,[a] Zhengxiao Ouyang,[a] Zhifeng Yu,[a] Tingting Tang,[a] Zhenan Zhu,[a] Xinhua Qu,[a] Kerong Dai[a]

Shanghai Key Laboratory of Orthopaedic Implants, Department of Orthopaedic Surgery, Shanghai Ninth People's Hospital, Shanghai Jiaotong University School of Medicine, Shanghai, China[a]; Department of Orthopaedic Surgery, the Central Hospital of Xuzhou, Xuzhou Clinical School of Xuzhou Medical College, Xuzhou Hospital (affiliated with Medical College of Southeast University), Jiangsu, China[b]; Department of Plastic and Reconstructive Surgery, Shanghai Ninth People's Hospital, Shanghai Jiaotong University School of Medicine, Shanghai, China[c]; Institute of Metal Research, Chinese Academy of Sciences, Shenyang, China[d]

Periprosthetic infection remains a challenging clinical complication. We investigated the antibacterial properties of pure (99.9%) magnesium (Mg) *in vitro* and in an *in vivo* rat model of implant-related infection. Mg was highly effective against methicillin-resistant *Staphylococcus aureus*-induced osteomyelitis and improved new peri-implant bone formation. Bacterial *icaA* and *agr* RNAIII transcription levels were also assessed to characterize the mechanism underlying the antibacterial properties of the Mg implant.

Artificial metal implants are widely used to repair bone injury due to fractures, tumor resection, and other causes. However, periprosthetic infections (PPI) are a clinically challenging complication, as the biomaterial implant surfaces serve as substrates for bacterial adhesion, colonization, and biofilm formation (1, 2). Prolonged antimicrobial treatment, implant removal, and surgical revision are often necessary to cure PPI, which leads to increased patient morbidity and places a substantial health care burden on society. Conventional PPI prevention relies on systemic antibiotics, which possess several disadvantages: (i) it is difficult to achieve an effective local antibiotic concentration without risking systemic toxicity, (ii) therapy is ineffective once the adherent bacteria have formed a biofilm on the implant surface, and (iii) they increase the emergence of antibiotic-resistant bacteria, such as methicillin-resistant *Staphylococcus aureus* (MRSA), a common osteomyelitis-inducing pathogenic bacterium. Thus, many studies have focused on the development of novel medical biomaterials with antibacterial properties, such as metal implants, that prevent and/or treat implant-associated infection (3–6).

Pure magnesium plates were first introduced as orthopedic implants in 1907. Since then, this biodegradable magnesium-based metal and its alloy have been widely investigated for their utility as implant materials suitable for bone and cardiovascular applications due to their cytocompatibility and mechanical properties similar to those of natural bone (7–10). Previous investigations have found that the corrosion products of Mg degradation possess *in vitro* antibacterial function because they increase local alkalinity (11). These characteristics suggest that Mg-based metal could provide clinical utility as an orthopedic implant to prevent implant-associated infections. We investigated the *in vitro* and *in vivo* antibacterial properties of pure Mg (99.9%) against MRSA. Rat models of implant-related osteomyelitis (Sprague-Dawley rats) were implanted with pure Mg intramedullary nails. The efficacy of the nails for treating osteomyelitis and the amount of new peri-implant bone formation were evaluated. We also assessed bacterial *icaA* and *agr* RNAIII transcription to identify the mechanism underlying the antibacterial properties of pure Mg.

The *in vitro* antibacterial efficiency of Mg and titanium (Ti) sample discs (ϕ = 15 mm) was analyzed using the spread plate method (12, 13) after coculturing with MRSA (ATCC 43300) for 6, 12, and 24 h. Adherent bacteria were removed from the sample surfaces and recultured on BBL tryptone soy agar (TSA), then quantified by colony counting (data expressed in CFU). The Ti surfaces served as positive controls. After 24 h, the pure Mg surfaces exhibited the lowest levels of MRSA colonization (Fig. 1A) and exhibited bactericidal efficiency in comparison to Ti ($P < 0.01$) (Fig. 1B).

Bacterial adherence and biofilm formation were analyzed by confocal laser-scanning microscopy (CLSM) (Leica TCS SP2; Leica Microsystems, Heidelberg, Germany) and field-emission scanning electron microscopy (FESEM) (Hitachi S-4800, CamScan) (Fig. 1C and D). The discs were stained with combination dye (LIVE/DEAD BacLight bacterial viability kits, catalog no. L13152; Molecular Probes) and observed by CLSM over time (Fig. 1C). Intense fluorescence on the Ti surfaces indicated a high level of biofilm formation, while pure Mg yielded fewer and smaller viable colonies. Twenty-four hours after coculture with MRSA, FESEM imaging of the Ti surfaces showed extensive colonization by spherical MRSA encased in a matrix suggestive of biofilm formation (Fig. 1D, Ti). In contrast, the Mg surfaces had only isolated, irregularly shaped individual bacteria (Fig. 1D, Mg).

Received 29 July 2014 **Returned for modification** 5 September 2014
Accepted 28 September 2014

Published ahead of print 6 October 2014

Address correspondence to Xinhua Qu, xinhua_qu@126.com, or Kerong Dai, krdai@163.com.

Yang Li, Guangwang Liu, Zanjing Zhai, and Lina Liu contributed equally to this work.

doi:10.1128/AAC.03936-14

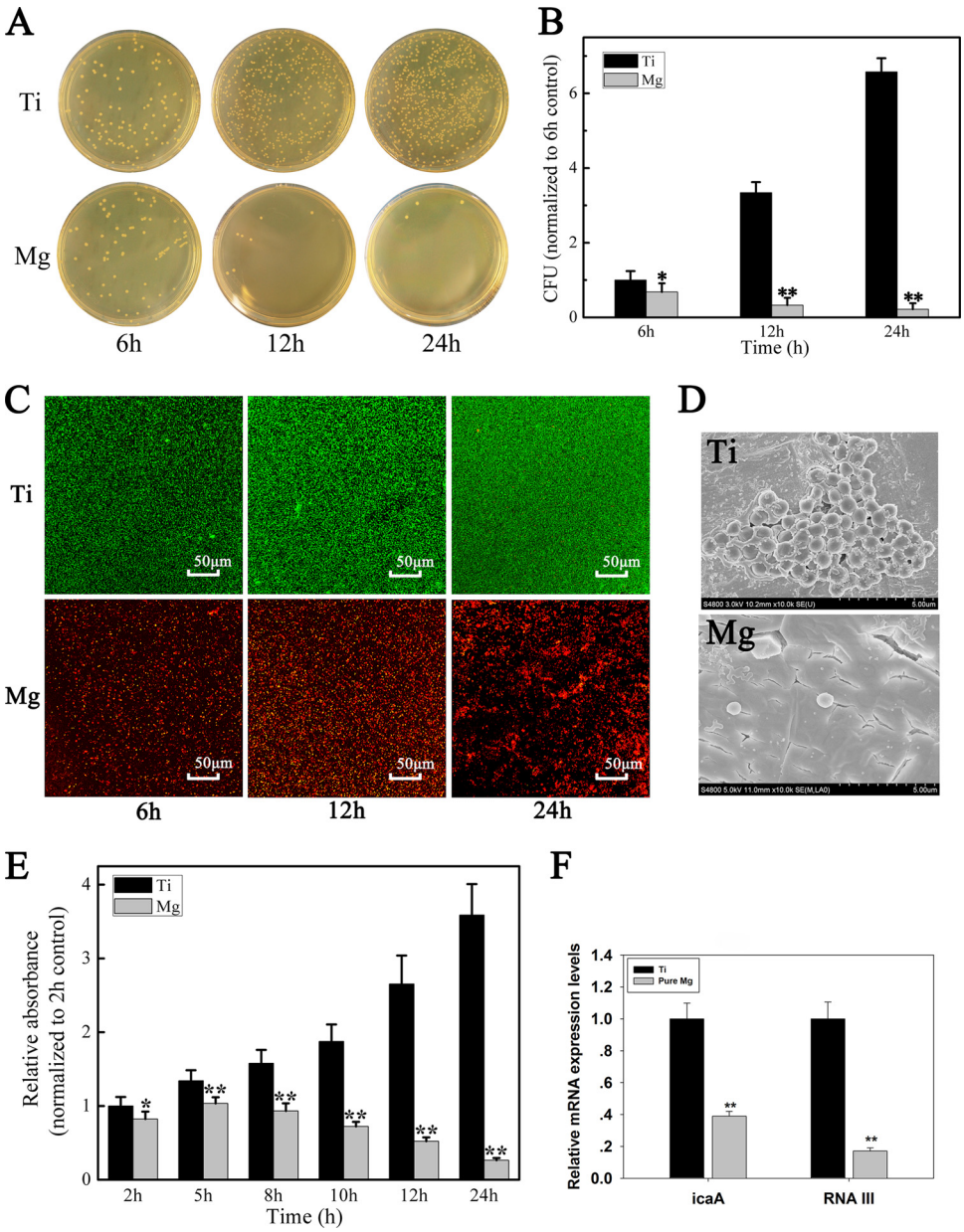

FIG 1 (A) Representative images of viable bacteria grown on different samples after 6, 12, and 24 h of culture. (B) The number of viable bacteria were counted and normalized to the number of bacteria on Ti samples. (C) CLSM images of bacteria adhered to the samples after 6, 12, and 24 h of culture. Bacteria are stained with green fluorescent SYTO 9 and red fluorescent propidium iodide, which cause living cells to appear green and dead cells to appear red under CLSM. (D) FESEM images of bacteria adhered to the samples after 24 h of culture. (E) Absorption of crystal violet was used as an indicator of biofilm formation by MRSA after 2, 5, 8, 10, 12, and 24 h of culture. The relative absorption of crystal violet was normalized to that of the 2-h control. (F) Expressions of the *icaA* and *agr* RNAIII genes were analyzed using real-time PCR. RNA transcription levels were normalized to the expression of bacteria on the Ti samples. Values are means ± standard deviation (SD). *, $P < 0.05$; **, $P < 0.01$.

Biofilms were stained with crystal violet according to the method of O'Toole et al. (14) (Fig. 1E). Sample surfaces were cocultured with MRSA for 2, 5, 8, 10, 12, and 24 h and then stained with crystal violet (Sigma-Aldrich, St. Louis, MO, USA) and solubilized in 95% ethyl alcohol (EtOH). Absorbance was measured at 570 nm using an automated plate reader (PerkinElmer). As expected, staining intensity was significantly higher on the Ti discs than on the Mg discs (Fig. 1E), indicating that pure Mg prevented MRSA biofilm formation.

Staphylococcal biofilm formation depends on synthesis of the polysaccharide intercellular adhesin (PIA), encoded by *icaA* (15–17). We examined *icaA* gene expression as an index of biofilm formation on Mg and Ti sample surfaces. Real-time PCR results showed that *icaA* was significantly downregulated in MRSA cultured with Mg versus that with Ti ($P < 0.01$) (Fig. 1F). We assume that this inhibition of *icaA* transcription resulted in the downregulation of PIA production, thereby reducing biofilm formation. We also measured the expression of the *Staphylococcus au-*

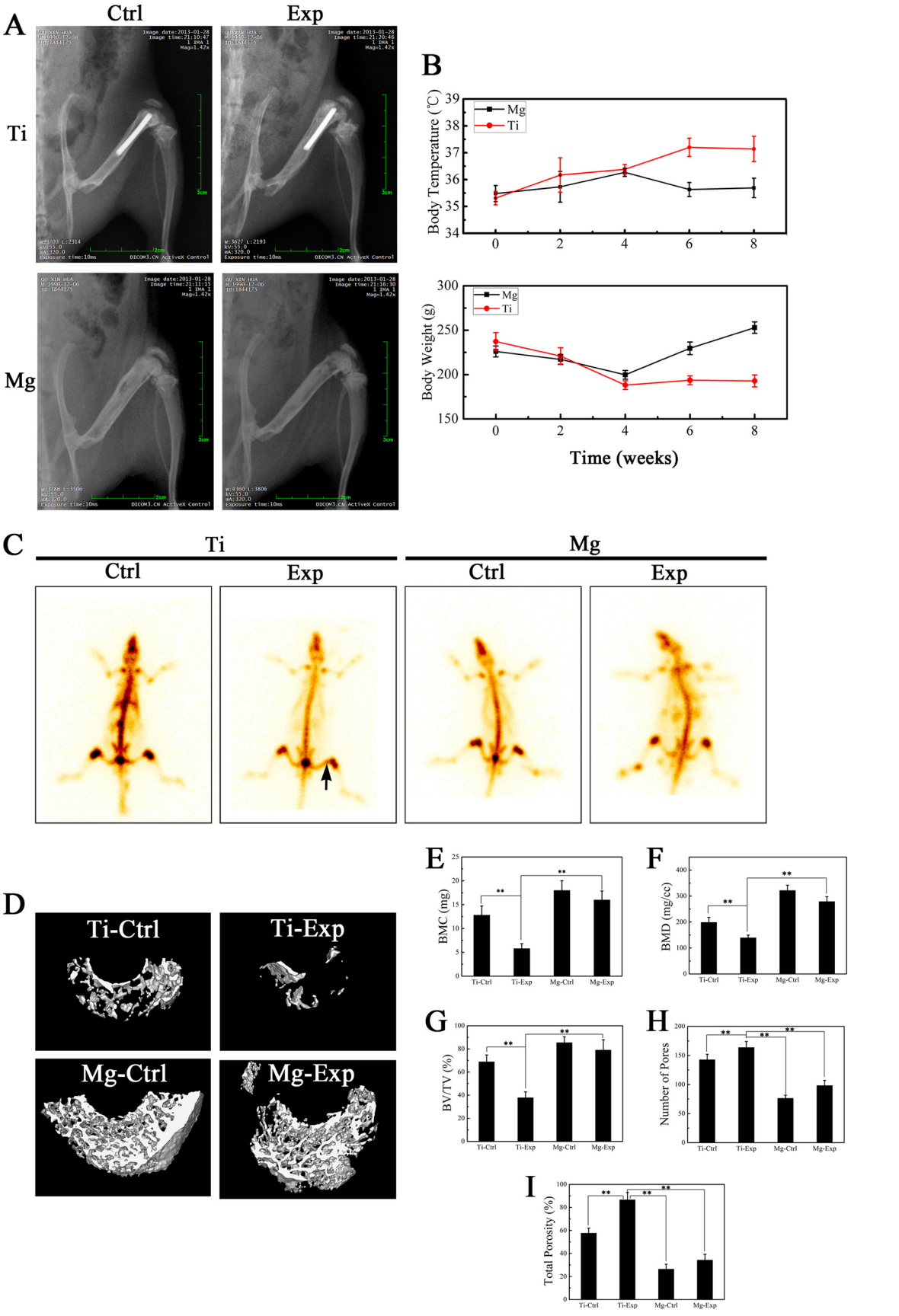

FIG 2 (A) X-ray digital films in posterior-anterior view of four rat groups 8 weeks after surgery. (B) Changes in body weight and temperature of animals. (C) ^{99m}Tc radioactivity emission computerized tomographic (ECT) images of four rat groups 8 weeks after surgery. (D) Representative micro-computerized tomography (CT) 3D reconstructed images obtained for each group. Bone mineral content (BMC) (E), bone mineral density (BMD) (F), body volume/tissue volume (BV/TV) (G), number of pores (H), and the percentage of total porosity (I) of each group sample were analyzed. Values are means ± SD. *, $P < 0.05$; **, $P < 0.01$.

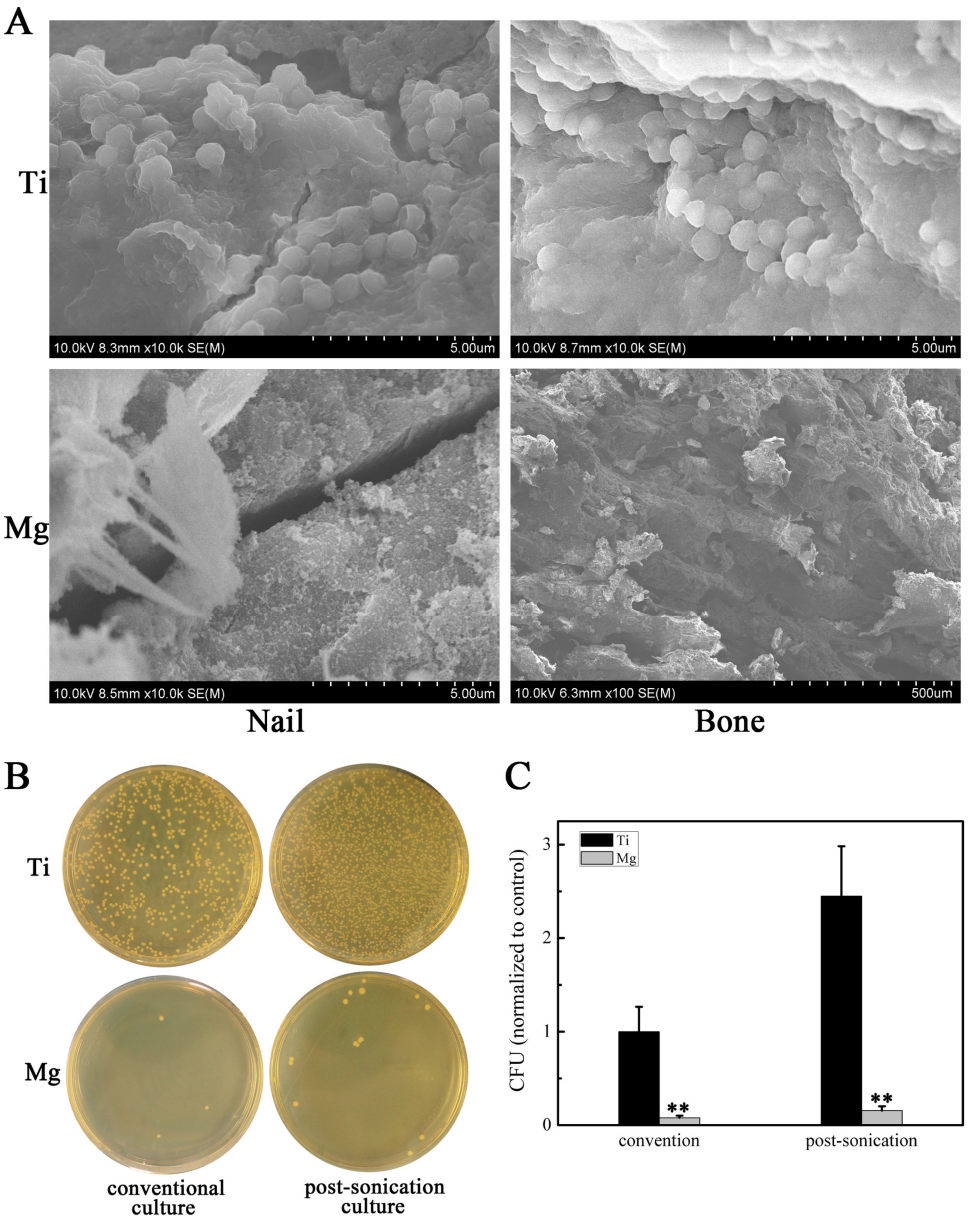

FIG 3 (A) FESEM images of Mg and Ti nails and bone tissue around implants. (B) Representative images of viable bacterial cultures of peri-implant bone tissues and implanted nails using the conventional or sonication method, respectively. (C) The number of viable bacteria in the Mg group were counted and normalized to the number of bacteria in the Ti group. Values are means ± SD. *, $P < 0.05$; **, $P < 0.01$.

reus accessory gene regulator RNAIII (*agr* RNAIII) in MRSA cocultures with Ti and Mg surfaces. The *agr* RNAIII locus regulates the production of several exoproteins and cell surface-associated proteins (18, 19). Regassa and Betley (18) found that alkaline pH represses the expression of *agr* RNAIII, consistent with our findings, in which *agr* RNAIII expression was significantly downregulated by coculturing with pure Mg ($P < 0.01$) (Fig. 1F). This result supports our hypothesis that the *in vitro* antibacterial property of Mg implants may be due to the increase in local alkalinity caused by Mg degradation.

In vivo, the right femur cavities of 5-month-old Sprague-Dawley rats were implanted with pure Mg and Ti intramedullary nails ($\phi = 1.5$ by 15 mm), which were precultured with MRSA (1×10^6 CFU/ml) for 24 h to induce implant-related osteomyelitis. These animals were designated the Mg and Ti experimental groups (Mg Exp and Ti Exp). Animals implanted with sterilized Mg and Ti nails were included as negative controls (Mg Ctrl and Ti Ctrl). Body temperatures remained stable in the Mg Exp animals but increased in the Ti Exp group during the follow-up period (Fig. 2B). Body weight decreased slightly in all groups during the first 4 weeks, but this was followed by a continuous weight gain in the Mg Exp group (Fig. 2B). Digital X-ray images of the posterior-anterior view were taken 8 weeks after surgery (Fig. 2A). The images showed osteomyelitis in the Ti Exp group, with bone destruction and new periosteal bone formation that were clearly worse than in the other three groups (Fig. 2A). There was no significant

difference between the Mg Exp and Mg Ctrl groups (Fig. 2A). Consistent with these results, an area of concentrated ^{99m}Tc radioactivity was observed by emission computerized tomography (ECT) in the distal femur of Ti Exp animals (Fig. 2C, black arrow). This suggested local infection; there was no abnormal radiation uptake in the other three groups. These results suggest that the Mg implant can effectively protect the bone and surrounding tissues from MRSA infection.

It is noteworthy that new peri-implant bone formation was observed in the Mg Exp and Mg Ctrl groups (Fig. 2A). Qualitative and quantitative evaluation of new peri-implant femoral bone formation was analyzed by high-resolution micro-CT (Skyscan 1072; Skyscan, Aartselaar, Belgium) (Fig. 2D) (20). The results showed high bone mineral density (BMD), bone mineral content (BMC), and body volume/tissue volume (BV/TV) and low total porosity and number of pores in the Mg Ctrl and Mg Exp groups versus the Ti Exp group ($P < 0.01$) (Fig. 2E to I). Quantification of bone parameters confirmed that Mg intramedullary nails prevent bone destruction induced by infection while promoting new bone formation around the implant.

Finally, we observed the implanted nails and surrounding bone tissue by FESEM and found that the Ti nail surfaces and bone tissue sites contained multiple bacterial colonies encased in a biofilm matrix (Fig. 3A). In contrast, virtually no bacteria were observed on the Mg nail surfaces and bone tissue (Fig. 3A). These results were confirmed by cultures of peri-implant bone tissues and implanted nails and analyzed by the conventional (21) and sonication (22) methods, respectively. Bacteria that were detached from the samples were recultured on TSA, and CFU were counted. MRSA growth was substantially inhibited on Mg nail surfaces and bone tissue sites compared to that on Ti nails (Fig. 3B and C).

We performed a systematic evaluation of the antibacterial properties of pure magnesium. The *in vitro* antibacterial assays demonstrated that an Mg implant reduced bacterial adhesion and prevented biofilm formation, most likely due to the increased local alkalinity caused by degradation of the metal. Implantation of an Mg intramedullary nail into the bone cavity of a rat protected the implant from bacterial contamination and improved new peri-implant bone formation. We suggest that biodegradable Mg-based biomaterials have a great potential for antibacterial orthopedic implant applications, to prevent and/or treat implant-associated infection, and thus to improve therapeutic efficacy and safety.

ACKNOWLEDGMENTS

This research was supported by grants from the Key National Basic Research Program of China (2012CB619101), the National Natural Science Foundation of China (81190133 and 81401852), the Natural Science Foundation of Science and Technology Commission of Shanghai Municipality (14ZR1424000), the Major Basic Research of Science and Technology Commission of Shanghai Municipality (11DJ1400303), the Clinical Medical Science and Technique Special Foundation of Jiangsu Provincial Department of Science and Technology (BL2014026), and the Xuzhou Medical Foundation for Youth Reserved Experts (2014006).

REFERENCES

1. **Romano CL, Manzi G, Logoluso N, Romano D.** 2012. Value of debridement and irrigation for the treatment of peri-prosthetic infections: a systematic review. Hip Int. **22**(Suppl 8):S19–S24. http://dx.doi.org/10.5301/HIP.2012.9566.
2. **Darouiche RO.** 2004. Treatment of infections associated with surgical implants. N. Engl. J. Med. **350:**1422–1429. http://dx.doi.org/10.1056/NEJMra035415.
3. **Kazemzadeh-Narbat M, Lai BF, Ding C, Kizhakkedathu JN, Hancock RE, Wang R.** 2013. Multilayered coating on titanium for controlled release of antimicrobial peptides for the prevention of implant-associated infections. Biomaterials **34:**5969–5977. http://dx.doi.org/10.1016/j.biomaterials.2013.04.036.
4. **Li Y, Liu YZ, Long T, Yu XB, Tang TT, Dai KR, Tian B, Guo YP, Zhu ZA.** 2013. Mesoporous bioactive glass as a drug delivery system: fabrication, bactericidal properties and biocompatibility. J. Mater. Sci. Mater. Med. **24:**1951–1961. http://dx.doi.org/10.1007/s10856-013-4960-z.
5. **Peng ZX, Tu B, Shen Y, Du L, Wang L, Guo SR, Tang TT.** 2011. Quaternized chitosan inhibits *icaA* transcription and biofilm formation by *Staphylococcus* on a titanium surface. Antimicrob. Agents Chemother. **55:**860–866. http://dx.doi.org/10.1128/AAC.01005-10.
6. **Jin G, Qin H, Cao H, Qian S, Zhao Y, Peng X, Zhang X, Liu X, Chu PK.** 2014. Synergistic effects of dual Zn/Ag ion implantation in osteogenic activity and antibacterial ability of titanium. Biomaterials **35:**7699–7713. http://dx.doi.org/10.1016/j.biomaterials.2014.05.074.
7. **Staiger MP, Pietak AM, Huadmai J, Dias G.** 2006. Magnesium and its alloys as orthopedic biomaterials: a review. Biomaterials **27:**1728–1734. http://dx.doi.org/10.1016/j.biomaterials.2005.10.003.
8. **Huehnerschulte TA, Reifenrath J, von Rechenberg B, Dziuba D, Seitz JM, Bormann D, Windhagen H, Meyer-Lindenberg A.** 2012. *In vivo* assessment of the host reactions to the biodegradation of the two novel magnesium alloys ZEK100 and AX30 in an animal model. Biomed. Eng. Online **11:**14. http://dx.doi.org/10.1186/1475-925X-11-14.
9. **Erbel R, Di Mario C, Bartunek J, Bonnier J, de Bruyne B, Eberli FR, Erne P, Haude M, Heublein B, Horrigan M, Ilsley C, Bose D, Koolen J, Luscher TF, Weissman N, Waksman R, PROGRESS-AMS Investigators.** 2007. Temporary scaffolding of coronary arteries with bioabsorbable magnesium stents: a prospective, non-randomised multicentre trial. Lancet **369:**1869–1875. http://dx.doi.org/10.1016/S0140-6736(07)60853-8.
10. **Witte F, Feyerabend F, Maier P, Fischer J, Stormer M, Blawert C, Dietzel W, Hort N.** 2007. Biodegradable magnesium-hydroxyapatite metal matrix composites. Biomaterials **28:**2163–2174. http://dx.doi.org/10.1016/j.biomaterials.2006.12.027.
11. **Robinson DA, Griffith RW, Shechtman D, Evans RB, Conzemius MG.** 2010. *In vitro* antibacterial properties of magnesium metal against *Escherichia coli*, *Pseudomonas aeruginosa* and *Staphylococcus aureus*. Acta Biomater. **6:**1869–1877. http://dx.doi.org/10.1016/j.actbio.2009.10.007.
12. **Tan H, Peng Z, Li Q, Xu X, Guo S, Tang T.** 2012. The use of quaternised chitosan-loaded PMMA to inhibit biofilm formation and downregulate the virulence-associated gene expression of antibiotic-resistant *Staphylococcus*. Biomaterials **33:**365–377. http://dx.doi.org/10.1016/j.biomaterials.2011.09.084.
13. **Wu T, Hua X, He Z, Wang X, Yu X, Ren W.** 2012. The bactericidal and biocompatible characteristics of reinforced calcium phosphate cements. Biomed. Mater. **7:**045003. http://dx.doi.org/10.1088/1748-6041/7/4/045003.
14. **O'Toole GA, Pratt LA, Watnick PI, Newman DK, Weaver VB, Kolter R.** 1999. Genetic approaches to study of biofilms. Methods Enzymol. **310:**91–109. http://dx.doi.org/10.1016/S0076-6879(99)10008-9.
15. **Arciola CR, Campoccia D, Baldassarri L, Donati ME, Pirini V, Gamberini S, Montanaro L.** 2006. Detection of biofilm formation in *Staphylococcus epidermidis* from implant infections: comparison of a PCR-method that recognizes the presence of *ica* genes with two classic phenotypic methods. J. Biomed. Mater. Res. A **76:**425–430. http://dx.doi.org/10.1002/jbm.a.30552.
16. **Rohde H, Frankenberger S, Zahringer U, Mack D.** 2010. Structure, function and contribution of polysaccharide intercellular adhesin (PIA) to *Staphylococcus epidermidis* biofilm formation and pathogenesis of biomaterial-associated infections. Eur. J. Cell Biol. **89:**103–111. http://dx.doi.org/10.1016/j.ejcb.2009.10.005.
17. **Arciola CR, Baldassarri L, Montanaro L.** 2001. Presence of *icaA* and *icaD* genes and slime production in a collection of staphylococcal strains from catheter-associated infections. J. Clin. Microbiol. **39:**2151–2156. http://dx.doi.org/10.1128/JCM.39.6.2151-2156.2001.
18. **Regassa LB, Betley MJ.** 1992. Alkaline pH decreases expression of the accessory gene regulator (*agr*) in *Staphylococcus aureus*. J. Bacteriol. **174:**5095–5100.
19. **Hild N, Tawakoli PN, Halter JG, Sauer B, Buchalla W, Stark WJ, Mohn D.** 2013. pH-dependent antibacterial effects on oral microorganisms through pure PLGA implants and composites with nanosized bioactive

glass. Acta Biomater. **9:**9118–9125. http://dx.doi.org/10.1016/j.actbio.2013.06.030.

20. **Wedemeyer C, Xu J, Neuerburg C, Landgraeber S, Malyar NM, von Knoch F, Gosheger G, von Knoch M, Loer F, Saxler G.** 2007. Particle-induced osteolysis in three-dimensional micro-computed tomography. Calcif. Tissue Int. **81:**394–402. http://dx.doi.org/10.1007/s00223-007-9077-2.
21. **Lucke M, Schmidmaier G, Sadoni S, Wildemann B, Schiller R, Haas NP, Raschke M.** 2003. Gentamicin coating of metallic implants reduces implant-related osteomyelitis in rats. Bone **32:**521–531. http://dx.doi.org/10.1016/S8756-3282(03)00050-4.
22. **Trampuz A, Piper KE, Jacobson MJ, Hanssen AD, Unni KK, Osmon DR, Mandrekar JN, Cockerill FR, Steckelberg JM, Greenleaf JF, Patel R.** 2007. Sonication of removed hip and knee prostheses for diagnosis of infection. N. Engl. J. Med. **357:**654–663. http://dx.doi.org/10.1056/NEJMoa061588.